Nonlinear resonance study of the periodic motion of the explosive crystallization front in glasses

Valerij A. Shklovskij and Vladimir N. Ostroushko
National Science Center, Kharkov Institute of Physics & Technology, 1 Akademicheskaya Street, Kharkov 310108, Ukraine
(Received 22 June 1995)

The theoretical treatment of self-sustained periodic motion of the explosive crystallization (EC) front in a thin amorphous film is presented. The main attention is given to the study of nonlinear resonance phenomena occurring due to the presence of a small external periodic perturbation with the frequency being in the vicinity of the ordinary or parametric resonance. Weakly anharmonic oscillations of the EC front velocity are considered with the Van der Pole method, and the expressions for the limit cycle amplitude in the case of free and forced oscillations are derived. Depending on the values of kinetic and thermophysical parameters of the model, different kinds of resonance curves (i.e., front oscillation amplitudes versus frequency detuning) are obtained and analyzed. Our predictions may be tested experimentally by monitoring the explosive growth rate using the modulation of laser intensity or employing amorphous films with thickness periodicity. It is also shown that inclusion of the results of dynamic stability analysis changes the steady-state EC stability diagram in the (T_s,d) plane (T_s is the substrate temperature and d the film thickness) so that the region of stable EC regimes becomes substantially more limited.

I. INTRODUCTION

It is well known that in the case of slow (''oven'') heating of glasses they all become crystallized at some temperature. This temperature depends relatively weakly on the heating rate as long as the rate of dissipation of the crystallization heat is high and we can ignore the influence of this rate on a possible self-acceleration of the slow decay process. However, this self-acceleration becomes possible if the heat removal is sufficiently slow.[1] Then the rapid production of the latent heat of crystallization at the boundary between the two phases (if experiments are designed properly) may result in a considerable self-acceleration of the phase transformation front. The front acquires the form of a thermal domain moving at a velocity of up to several tens of meters per second. The motion of the crystallization front in this regime is defined as explosive. So the specific feature of a nonisothermic one-dimensional amorphous-crystalline phase transformation is the possibility, under identical external conditions, of two different steady-state regimes of crystallization, namely, slow and explosive, which are chosen by the system according to the initial conditions. A detailed analysis of theoretical and experimental aspects of self-sustained quasisteady explosive crystallization (EC) of glasses has been made in the review Ref. 2. It also gave a brief discussion of some nonstationary effects, mainly from the viewpoint of a linear stability analysis of the steady-state solution of one-dimensional EC front propagation. The analysis revealed[3,4] that under certain conditions the steady state can undergo a Hopf bifurcation, so that the EC front actually advances with an oscillating velocity. The existence of this self-sustained oscillatory instability even for a homogeneous amorphous film implies that, in the presence of an external driving force with the frequency in the neighborhood of harmonics of self-sustained oscillations of the EC front, we can expect a great variety of resonant phenomena, well known in nonlinear dynamics.[5,6]

The aim of this paper is to investigate theoretically the nonlinear resonant phenomena which can occur during EC front propagation in the presence of small external periodic perturbations. For simplicity, we restrict our consideration to the straight-line front and discuss separately only two types of such perturbations, namely, those with time and space periodicities. In the first case, the experimental realization is associated with time modulation of the intensity of a uniformly moving laser slit (see Fig. 1) in the process of so-called laser-driven EC (see the important paper on this subject by Kurtze, van Saarloos, and Weeks[7]). Spatial periodicity of the external driving force can be realized experimentally for specially prepared thin amorphous films with spatially modulated thickness (see Fig. 2). Such films can be prepared, for example, by making wavy the surface of the substrate before film deposition. As we shall see below, from the qualitative viewpoint the resonant behavior of the EC front propagation is similar for the both cases. However, since the time modulation of laser intensity appears a simpler way to study by experiment the resonant phenomena under discussion, below we pay the main attention to this particular case.

Let us now briefly summarize at a qualitative level the main features and some results of our approach. Formally, the system considered, due to the possibility of heat diffusion, has an infinite number of degrees of freedom and, in

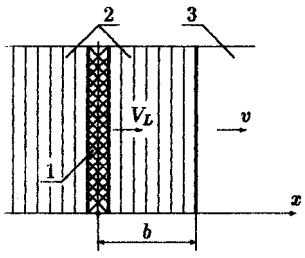

FIG. 1. Laser-driven crystallization: 1, laser slit, 2, crystalline region, 3, amorphous region; V_L is the velocity of the laser slit, v is the crystallization front velocity, and b is the average distance between the front and the laser slit.

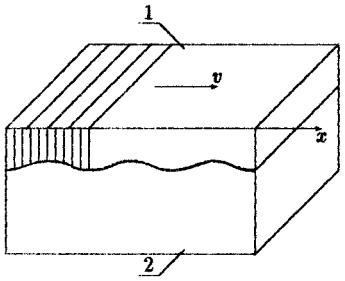

FIG. 2. Crystallization of amorphous film having varying thickness: 1, film; 2, substrate.

general, the dynamics of an amorphous-crystalline (A-C) interface coordinate $s(t)$ is described by a highly complicated integral equation. It is very important, however, that there exists a special surface in the space of some dimensionless parameters of the system (α, β, and R, see Sec. II below) where the oscillatory solution for the front velocity $v(t)\equiv\dot{s}(t)$ exists in the form $v(t)\sim\exp(i\omega_0 t)$ with $0<\omega_0<\infty$ and zero damping (in the linear approximation with respect to a small perturbation). Moreover, near the above line we can consider oscillations having a small but finite growth factor κ_0 ($\kappa_0>0$) as well as ones having a small damping factor $-\kappa_0$ (if $\kappa_0<0$) (in both cases $|\kappa_0|\ll\omega_0$).

Thus, for finite but small deviations in the amplitude of $v(t)$ oscillations, we can represent our system as the usual[5] nonlinear one-dimensional oscillator with unperturbed frequency ω_0 and "damping" $-\kappa_0$. There is only one essential distinction as compared with the usual case, namely, the unperturbed "damping" is not a constant but a rather complicated function of oscillator frequency ω and some other relevant parameters. As a consequence, the "damping," depending on those parameters, may be either positive (and associated with a real damping of oscillations) or negative, which corresponds to the growth of oscillations.

Even in the absence of an external force, the consideration of nonlinearity leads to qualitatively new features of the oscillator behavior, especially important in the case of $\kappa_0>0$. Within the framework of the Van der Pole method[8] one can search for small nonlinear oscillations in the form of an expansion, where the first term gives the main harmonic oscillation of a small (unknown yet) amplitude $s_1\equiv a$ with a frequency $\omega(a)$ and a growth factor $\kappa(a)$, which are, in turn, the sums of different-order terms in a itself. The equations for determining higher-order terms contain the products of the first approximation terms; thus, in the calculations the displacement amplitude values $s_0, s_2, \ldots, s_n, \ldots$ of zero, second and, in general, higher harmonics appear. These amplitudes, in turn, may be determined after the substitution of the $s(t)$ expansion into the initial integral equation of the problem by comparing the terms proportional to the same power of a in the expansion obtained (see Secs. III and V for details of calculations).

In the following we consider a very important case, where not only the main harmonic amplitude a is small, but our nonlinear oscillations also have a slowly varying amplitude, i.e., $|\dot{a}|\ll a\omega$, which corresponds to $|\kappa_0|\ll\omega_0$. Then we can restrict our multifrequency expansion to only second- and zero-harmonic terms. In this so-called "quasiharmonic" approximation[8] the lowest nonlinear correction to the amplitude of the second harmonic s_2 is proportional to a^2

$$s_2=\tilde{B}_2 a^2, \tag{1.1}$$

and the main correction to s_1 is proportional to a^3. The corrections to the unperturbed frequency ω_0 and the growth factor κ_0 in the lowest approximation are also proportional to a^2, i.e.,

$$\omega(a)=\omega_0-\mu a^2, \quad \kappa(a)=\kappa_0-\chi a^2, \tag{1.2}$$

where χ and μ [as well as $\tilde{B}_2$ in (1.1)] should be defined self-consistently by the perturbation expansion of the front velocity $v(t)$ as a function of the relevant parameters.

Taking into account relations (1.2) we can show that, if κ_0 is small and positive (the case of growing unperturbed oscillations), then for $\chi>0$ the limit cycle $\kappa(a)=0$ with the amplitude $a=a_0$ is possible, where

$$a_0=\sqrt{\kappa_0/\chi}. \tag{1.3}$$

Since $\kappa_0>0$ in this case, and we have $\kappa>0$ for $a<a_0$, the excitation of the limit cycle is possible for arbitrarily small values of a, if κ_0 is sufficiently small.

In the opposite case, $\kappa_0<0$ and $\chi<0$, in the linear approximation the oscillations of the front with amplitude $a=a_0$ (1.3) are unstable: if $a<a_0$, then $\kappa(a)<0$, so the oscillations decay, but if $a>a_0$ the oscillations will grow, and then the quasiharmonic consideration cannot describe their further evolution.

Essentially new features also appear with the inclusion of nonlinearity in the case of forced oscillations, especially in the resonance regime. As is known,[5] in the linear approximation, the response a of a weakly forced oscillator near the resonance frequency is proportional to the product $f(\delta^2+\kappa_0^2)^{-1/2}$, or, in another way,

$$a^2(\delta^2+\kappa_0^2)=f^2, \tag{1.4}$$

where the detuning $\delta=\nu-\omega_0$ is the difference between the frequency ν of the external force f and the unperturbed frequency ω_0, and κ_0 is assumed to be negative.

Taking account of nonlinearity changes this formula so that ω_0 and κ_0 gain the small amplitude corrections given by formula (1.2). Substituting (1.2) into (1.4) we obtain the equation which generalizes formula (1.4) for the nonlinear oscillator near resonance:[6]

$$a^2[(\delta+\mu a^2)^2+(\kappa_0-\chi a^2)^2]=f^2. \tag{1.5}$$

According to (1.5), the resonance system's behavior is similar to linear, if the external force is small. When its amplitude exceeds some critical value, the resonance curve (dependence of the oscillation amplitude upon the value of the external-force frequency detuning at a fixed external-force amplitude) changes so that an ambiguity interval appears,[5] i.e., each frequency value corresponds to three oscillation amplitude values [see Fig. 3(b) below]. The intermediate part of the curve corresponds to unstable oscillations, so in some frequency range there exist two possible values of the stable oscillation amplitude. One of them may be obtained with a decrease in frequency and the other with its increase, and as the frequency reaches its definite value the oscillation ampli-

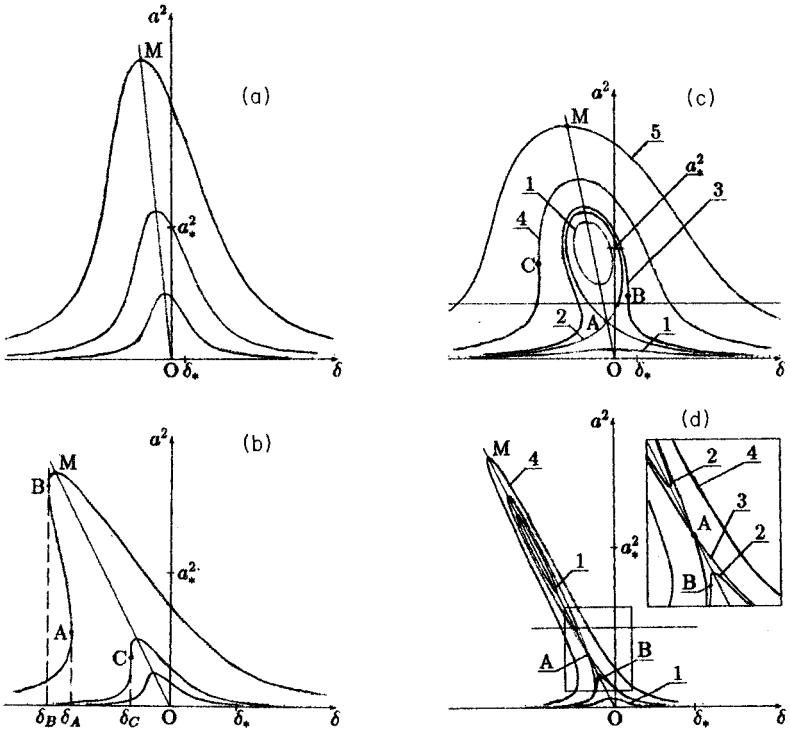

FIG. 3. The squared oscillation amplitude a^2 (3.1) as a function of detuning δ (resonance curves) for the case of ordinary resonance. The cases (a)–(d) correspond to different relationships between κ_0, χ, and μ (1.2), and the curves in each subfigure correspond to different values of the renormalized external-force amplitude f (3.18). (a) The case $\kappa_0\chi<0$, $\mu^2<3\chi^2$ [$(\mu/\chi)^2=1$ for the curves]. For the curves the f/f_2 ratio (4.2) is equal to 2.76, 5.86, and 12.67, respectively, in order of increasing maximal a^2 (in the curve). (b) The case $\kappa_0\chi<0$, $\mu^2>3\chi^2$ [$(\mu/\chi)^2=25$]. For the curves the f/f_2 ratio is approximately equal to 1.62, 2.78, and 9.45, respectively, in the mentioned order. Point C and points A and B with vertical tangents lie in the curves with $f=f_3$ (4.1) and $f>f_3$, respectively. (c) The case $\kappa_0\chi>0$, $\mu^2<3\chi^2$ [$(\mu/\chi)^2=0.111$]. For curves 1, 2, 3, 4, and 5 the f/f_2 ratio is approximately equal to 0.71, 1.0, 1.14, 2.05, and 4.14, respectively. For $f=f_2$ (4.2) the branches link at point A. Points B and C with vertical tangents lie in the lower branch of the curves with $f=f_1$ (4.3) and $f=f_3$, respectively. (d) The case $\kappa_0\chi>0$, $\mu^2>3\chi^2$ [$(\mu/\chi)^2=25$]. For curves 1, 2, 3, and 4 the f/f_2 ratio is approximately equal to 0.61, 0.94, 1.0, and 1.83, respectively. For $f=f_2$ the branches link at point A. Point B with vertical tangent lies in the lower branch of the curve with $f=f_1$. The horizontal line indicates the stability boundary (4.6). The natural units along the axes $a_*^2=|\kappa_0/\chi|$ and $\delta_*=|\mu\kappa_0/\chi|$ are marked on the axes.

tude changes discontinuously, so that the point which indicates the system's state jumps to another part of the resonance curve.

In contrast to the common nonlinear oscillator,[5] in the system considered the inclusion of nonlinearity implies the dependence of not only the resonance frequency but also the growth factor κ upon the external-force amplitude [see formula (1.5)]. The two dependences are square with respect to the amplitude. For a certain relationship between the coefficients in those dependences, the resonance curve broadening (with the amplitude growth) compensates the curve bending, so that the interval of ambiguity does not arise [see Fig. 3(a)]. For the other relationship between μ and χ this interval may arise. If the growth factor decreases with the amplitude growth, the interval of the external force amplitude for which the oscillation amplitude ambiguity takes place does exist, but it may be restricted. In addition, for a sufficiently small external force, the resonance curve is divided into two parts: the lower branch may be obtained from the linear analysis, while the upper [a closed loop, see Figs. 3(c) and 3(d)] is the result of nonlinearity. In particular, if the external force is absent, the curve consists of a straight line (zero amplitude) and a point; the last corresponds to self-sustained oscillations.

If the external perturbation frequency is close to double that of the self-sustained oscillations, then the case of parametric resonance is realized. It has some features of the above-described ordinary resonance, in particular, intervals of bistability [Figs. 4(a) and 4(b)]. But in this case the external force at the main harmonics becomes proportional to a^2, so that the factor a^2 cancels out in the left and the right sides of the equation analogous to (1.5), and we arrive at the square equation with respect to a^2 [see (3.25) below]. As a result, an essential realization of the parametric resonance requires the external perturbation amplitude to be proportional to the damping, that is, to be greater than that for the ordinary resonance, which is proportional to damping to the power $1\frac{1}{2}$.

In the next section we review the model used in Refs. 3 and 4 and the results of its linear stability analysis in the form presented by van Saarloos and Weeks[4] (directly relevant to this paper), and also discuss in detail possible ways of introducing the external oscillatory force into the basic equation for EC front propagation. In Sec. III, we outline the main steps of the Van der Pole method as applied to the study of periodic motion of the laser-driven EC front. The results of nonlinear resonance treatment are presented in Sec. IV. In Sec. V, the case of spatial inhomogeneity of heat removal is

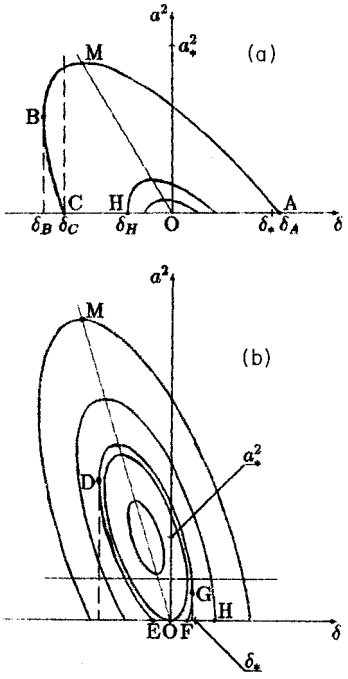

FIG. 4. Resonance curves for the case of parametric resonance. The cases (a) and (b) correspond to different signs of the product of the initial increment κ_0 by the coefficient χ in its dependence upon the amplitude (1.2), and the curves in each subfigure correspond to different values of the renormalized external-force amplitude g (3.24). The curves are the ellipses (or their parts) with center at the point $a^2=\kappa_0/\chi$, $\delta=-\mu\kappa_0/\chi$, and the greater g, the greater is the ellipse size. (a) The case $\kappa_0\chi<0$. For the curves the g/g_0 ratio (4.4) is approximately equal to 1.08, 1.2, and 1.9, respectively. All the curves have $g>g_0$. The curve with $g=g_1$ (4.5) has the vertical tangent at the point H on the axis $a^2=0$. For any frequency in the interval (δ_B,δ_C) there are two values of the amplitude. (b) The case $\kappa_0\chi>0$. For the curves the g/g_0 ratio is approximately equal to 0.44, 1., 1.12, 1.67, and 2.6, respectively. The points D, E, F, and G lie on the curve with $g\in(g_0,g_1)$. For any frequency in the intervals (δ_D,δ_E) and (δ_F,δ_G) there are two corresponding values of the amplitude. For $g=g_0$ the curve is tangent with the axis $a^2=0$ at point O, and for $g=g_1$ the curve has a vertical tangent at point H on this axis. The units along the axes are the same as in Fig. 3.

considered as one of the alternative possibilities for a nonlinear resonance realization. In Sec. VI we discuss the EC stability diagram with consideration of the results of the linear stability analysis. The results of the paper and conclusions are summarized in Sec. VII.

II. REVIEW OF THE MODEL

Let us consider a straight boundary between amorphous and crystalline regions which moves across a thin, initially amorphous film. In the case of laser-driven explosive crystallization (see Fig. 1), the laser advances in the x direction at a fixed speed, driving the straight crystallization front ahead of it.[7] The commonly used theoretical model of EC, which was introduced by Gilmer and Leamy[1] and independently by one of the present authors,[3] incorporates heat diffusion (in the plane of the film) and heat sink to the substrate, latent heat release at the A-C boundary and interface kinetics of the A-C transition via a nonlinear dependence of the velocity of the boundary on its temperature. In the laboratory frame the local temperature of the film $T(x,t)$ obeys the one-dimensional equation

$$c\,\partial_t T(x,t)=\lambda\,\partial_x^2 T(x,t)-\Gamma[1-\gamma(x)][T(x,t)-T_s]+Lv(t)\,\delta(x-s(t))+[1+p(t)]P_0(x-l(t)).$$

Here $s(t)$ is the position of the phase boundary, $v(t)=ds(t)/dt$ is its velocity, T_s is the substrate temperature, λ, c, and L are the heat conductivity, the specific heat, and the latent heat of crystallization, respectively, ∂_t and ∂_x are the derivatives with respect to t and x, $l(t)$ is the coordinate associated with the laser slit and it is assumed that $dl(t)/dt=u=\text{const}$, $P_0(\xi)$ characterizes the unperturbed laser-power space distribution, $p(t)$ is its relative time modulation, Γ is the average coefficient of heat transfer to the substrate, and $\gamma(x)$ is its relative spatial inhomogeneity.

From this point on we introduce c/Γ, $\sqrt{\lambda/\Gamma}$, L/c, and $L\Gamma/c$ as units of time, coordinate, temperature, and power. In the new units, the equation may be written in the dimensionless form

$$\partial_t T(x,t)=\partial_x^2 T(x,t)-[1-\gamma(x)][T(x,t)-T_s]+v(t)\,\delta(x-s(t))+[1+p(t)]P_0(x-l(t)). \tag{2.1}$$

Equation (2.1) is incomplete unless the relation between the boundary velocity v and the front temperature $T(s(t),t)$ is specified. In our approach, the local interface velocity is determined by boundary temperature through the phenomenological relation

$$v(t)=V(T(s(t),t)), \tag{2.2}$$

where the function $V(T)$, being a property of the material, is regarded as given. It is generally assumed[2] that for crystallization from the amorphous phase $V(T)$ is an increasing function of the interface temperature and for theoretical estimates we can put

$$V(T)=V_s\,\exp(-E/T), \tag{2.3}$$

where $V_s=\text{const}$ and E is the activation energy in our temperature units (experimental values of E for different glasses can be found in Table 1 of Ref. 2). As pointed out earlier,[3,4,7] the fact that V is an increasing function of T with saturation at high temperatures makes the behavior of the EC process qualitatively different from the crystallization in a slightly undercooled liquid, where $dV/dT<0$ and the release of the heat of the transition hinders the crystallization process. In the case of amorphous materials we always have $dV/dT>0$ and the latent-heat release accelerates crystallization. Such a positive feedback and the activated nature of the decay of glasses (2.3) provide conditions for manifestation of the explosive-type thermal instability where relatively small changes of easily controlled parameters can greatly alter the rate of the crystallization process.

Equations (2.1) and (2.2) together with the boundary condition $T=T_s$ far from the A-C interface complete the specification of this highly nonlinear moving-boundary problem. By the use of the unperturbed Green function Eq. (2.1) may be rewritten in an integral form:

$$T(x,t)=T_s+\int_0^\infty d\tau\,\frac{v(t-\tau)}{2\sqrt{\pi\tau}}\exp\left\{-\tau-\frac{1}{4\tau}[x-s(t-\tau)]^2\right\}+\int_0^\infty d\tau\int_{-\infty}^{+\infty}d\eta\,\frac{1+p(t-\tau)}{2\sqrt{\pi\tau}}\,P_0(\eta)\exp\left\{-\tau-\frac{[x-l(t-\tau)-\eta]^2}{4\tau}\right\}+\int_0^\infty d\tau\int_{-\infty}^{+\infty}d\xi\,\frac{\gamma(\xi)[T(\xi,t-\tau)-T_s]}{2\sqrt{\pi\tau}}\exp\left\{-\tau-\frac{(x-\xi)^2}{4\tau}\right\}. \tag{2.4}$$

The first integral in the right-hand side deals with the heat release from the front, the second one with heat release from the laser slit, and the third one with the spatial inhomogeneity of heat removal. For $p=0$ and $\gamma=0$, Eqs. (2.4) and (2.2) have a steady-state solution, for which the temperature $T_f\equiv T(s(t),t)$ of interface and its position b_f with respect to the moving laser slit are determined for a given u by the set of equations

$$T_f=T_s+\Theta_c(u)+\Theta_l(0,u,b_f),\quad u=V(T_f),$$

where $\Theta_c(u)=(1+4u^{-2})^{-1/2}$,

$$\Theta_l(\nu,u,b_f)=\int_0^\infty\frac{d\tau\,e^{-i\nu\tau}}{2\sqrt{\pi\tau}}\int_{-\infty}^{+\infty}d\eta\;P_0(\eta)\exp\left[-\tau-\frac{(u\tau+b_f-\eta)^2}{4\tau}\right],$$

and the local temperature is calculated by

$$T(s(t)+\xi,t)=T_s+(T_f-T_s)\exp[-(u/2)\xi-|\xi|\sqrt{1+(u/2)^2}]+\Theta_l(0,u,b_f+\xi).$$

Following Ref. 7, it is useful to define the parameter $\beta\equiv\Theta_c^2(u)$, which ranges between 0 and 1 and can be considered as a dimensionless measure of the importance of heat loss, the parameter $\alpha\equiv(\sqrt{\beta}/u)[dV(T)/dT]_{V(T)=u}$, which measures the sensitivity of the front velocity to the interface temperature, and the parameter $R\equiv-2\partial_b\Theta_l(0,u,b)/(u\sqrt{\beta})$, which measures the laser influence. The linear stability equation has the form[7]

$$[i\Omega+\alpha(1+R)]\sqrt{1+2i\Omega\beta}=\alpha(1+i\Omega), \tag{2.5}$$

where Ω is the (complex) frequency multiplied by $2/u^2$. The surface in $\{\alpha,\beta,R\}$ space, where Ω is real, divides the space into regions where the straight-line front oscillations are, respectively, stable and unstable. This surface may be determined[7] with the formulas

$$\alpha=\frac{(1+R)(2q^2-1)-q}{(1+R)q-1},\quad \beta=\frac{q(q^2-1)}{(1+R)(2q^2-1)-q}, \tag{2.6}$$

where q is a parameter, $q>1$; and the Ω value at a point on the surface is given by

$$\Omega=[(1+R)(2q^2-1)-q]/\sqrt{q^2-1}.$$

The region $\kappa_0\ll\omega_0$ corresponds to points near the surface. The detailed nonlinear analysis carried out by Kurtze[9] deals with low-frequency oscillations, which take place if R is small. Our consideration deals with arbitrary frequencies but small amplitudes.

Mention should be made of a possible "morphological instability"[7] (for which the front is not a straight line) in the region where the straight-line front oscillations are stable. But the analysis made in Ref. 7 shows that for $q\in(1,1+R)$ the surface (2.6) is the true boundary between the regions of stable and unstable regimes.

III. NONLINEAR RESONANCE TREATMENT OF LASER-DRIVEN EXPLOSIVE CRYSTALLIZATION

We now consider the oscillations of the interface motion with a small slowly varying amplitude in the case of homogeneous heat removal [$\gamma(x)=0$]. The function $s(t)$ may be written as

$$s(t)=l(t)+b+\mathrm{Re}(ae^{i\varphi}+a^2\tilde{B}_2e^{2i\varphi}+\cdots). \tag{3.1}$$

Here Re denotes the "real part;" $a=a(t)$ and $\varphi=\varphi(t)$ are, respectively, the amplitude and the phase of the main mode; the growth factor $\kappa\equiv d\ln a/dt$ and the frequency $\omega\equiv d\varphi/dt$ of the main mode are supposed to be approximately constant, and $\kappa\ll\omega$, so that during one oscillation period the change in the amplitude is small; $b\approx b_0$, where b_0 is the root of a set of equations

$$T_0=T_s+\Theta_c(u)+\Theta_l(0,u,b_0),\quad u=V(T_0); \tag{3.2}$$

the factor $a^2\tilde{B}_2$ corresponds to the amplitude of the second harmonic of the relative front position oscillations (with respect to the laser slit), and for the average relative front position we may write

$$b=b_0+a^2\bar{B}_2+\cdots, \tag{3.3}$$

where the coefficient $\bar{B}_2$ (and also $\tilde{B}_2$) can be found from the harmonic balance [see (3.11) and (3.12) below]. The expansion (3.1) leads to the expansion

$$v(t)=\dot{s}(t)=u+\mathrm{Re}[(\kappa+i\omega)ae^{i\varphi}+2(\kappa+i\omega)a^2\tilde{B}_2e^{2i\varphi}+\cdots]. \tag{3.4}$$

If the oscillation amplitude a is small, for a disturbance of the form $p(t)=p\cos(\nu t)$ with small p, the expansion of the right-hand side of Eq. (2.4) yields

$$T(s(t),t)=p\;\mathrm{Re}[e^{i\nu t}\Theta_{l0}(\nu)+ae^{i(\nu t-\varphi)}\Theta_{l1}(\nu)]+\bar{T}+\mathrm{Re}\{ae^{i\varphi}[Q(\kappa+i\omega,u)+2\Theta_{l1}]+a^2e^{2i\varphi}\tilde{\Theta}_2+a^3e^{i\varphi}\tilde{\Theta}_3\}+\cdots, \tag{3.5}$$

$$\bar{T}=T_0+a^2\overline{\Theta}_2+\cdots, \tag{3.6}$$

where

$$\overline{\Theta}_2=\bar{A}_t+\Theta_{l2}+2\Theta_{l1}\bar{B}_2,$$

$$\tilde{\Theta}_3=\tilde{B}_2(\tilde{F}_3+2\Theta_{l2})+4\Theta_{l2}\bar{B}_2+\Theta_{l3}+\tilde{A}_3,$$

and

$$\tilde{\Theta}_2=\tilde{B}_2[Q(2i\omega,u)+2\Theta_{l1}]+\Theta_{l2}+\tilde{A}_2$$

are the proportionality coefficients, respectively, in the second-order correction to the average front temperature, in the third-order correction to the amplitude of the main mode of front temperature oscillations, and in the second harmonic of these oscillations.

$$Q(w,u)=\frac{1}{2}\left(\frac{u^2+2w}{\sqrt{4+u^2+4w}}-\frac{u^2}{\sqrt{4+u^2}}\right) \tag{3.7}$$

is the linear response of the front temperature to relative front position oscillations. $\Theta_{ln}(\nu)$ for integer n are the values of the function

$$\Theta_{ln}(\nu,u,b)=2^{-n}\partial_b^n\Theta_l(\nu,u,b)$$

at $b=b_0$, and the absence of the argument ν indicates that $\nu=0$ is supposed, so the parameters Θ_{ln} stem from the spatial derivatives of the stationary temperature profile determined by the laser heating, at the stationary front position. The expressions for $\bar{A}_t$, $\bar{A}_2$, $\tilde{F}_3$, and $\tilde{A}_3$ are given in the Appendix.

In (3.5) and (3.6) the terms of the main mode are kept up to a^3, the double-frequency and nonoscillating terms are kept up to a^2, and the terms responsible for the perturbation are kept to investigate the ordinary resonance at the main mode ($\nu=\omega$) and the parametric resonance ($\nu=2\omega$). Further, the expansion of the function $V(T)$ near the steady-state point, in view of Eq. (3.5), gives

$$V(T(s(t),t))=pV^{(1)}\mathrm{Re}[e^{i\nu t}\Theta_{l0}(\nu)+ae^{i(\nu t-\varphi)}\Theta_{l1}(\nu)]+u+a^2[V^{(1)}\overline{\Theta}_2+\tfrac{1}{4}V^{(2)}|Q+2\Theta_{l1}|^2]$$
$$+\mathrm{Re}\{ae^{i\varphi}V^{(1)}[Q(\kappa+i\omega,u)+2\Theta_{l1}]+a^3e^{i\varphi}\tilde{V}_3\}+\mathrm{Re}\{a^2e^{2i\varphi}[V^{(1)}\tilde{\Theta}_2+\tfrac{1}{4}V^{(2)}(Q+2\Theta_{l1})^2]\}+\cdots, \tag{3.8}$$

where the superscript in parentheses indicates the function derivative order at a steady-state value of the argument, $Q=Q(i\omega,u)$ [see formula (3.7)],

$$\tilde{V}_3=V^{(1)}\tilde{\Theta}_3+V^{(2)}[\tfrac{1}{2}\tilde{\Theta}_2(Q^*+2\Theta_{l1})+\overline{\Theta}_2(Q+2\Theta_{l1})]$$
$$+\tfrac{1}{8}V^{(3)}(Q+2\Theta_{l1})^2(Q^*+2\Theta_{l1}) \tag{3.9}$$

is the proportionality coefficient in the third-order correction to the amplitude of the main mode of the front velocity oscillations, and the asterisk denotes the complex conjugate.

As a consequence of (3.4) and (3.8), the weakly anharmonic oscillations considered would take place at b_0 and T_0 values [satisfying (3.2)] for which the equation

$$w=V^{(1)}(T_0)[Q(w,u)+2\Theta_{l1}(0,u,b_0)] \tag{3.10}$$

has the root $w=\kappa_0+i\omega_0$ with $\kappa_0\ll\omega_0$ (physically, κ_0 and ω_0 are the unperturbed values of the growth factor and frequency, respectively). If we introduce the parameter $\Omega\equiv 2w/(iu^2)$, Eq. (3.10) takes the form of the linear stability equation for laser-driven crystallization (2.5).

Further, comparison of the amplitudes of double-frequency terms and nonoscillating terms in (3.4) and (3.8) with neglect of real part of root of Eq. (3.10) yields

$$\overline{\Theta}_2=-(\omega_0/2)^2V^{(2)}[V^{(1)}]^{-3},$$
$$\bar{B}_2=(\overline{\Theta}_2-\bar{A}_t-\Theta_{l2})/(2\Theta_{l1}), \tag{3.11}$$

$$\tilde{B}_2=\frac{V^{(1)}(\Theta_{l2}+\tilde{A}_2)+\frac{1}{4}V^{(2)}(Q+2\Theta_{l1})^2}{2i\omega_0-V^{(1)}[Q(2i\omega_0,u)+2\Theta_{l1}]}. \tag{3.12}$$

These formulas, together with (3.1), (3.3), and (3.6), yield the corrections to the steady-state values and the double-frequency amplitude, if the main mode amplitude is given. Generally, $\tilde{B}_2$ is complex, so it contains the phase shift, too.

Let us now determine the main mode amplitude for the cases with and without a disturbance of laser heating. Let $p=0$ and κ_0 be a small positive quantity. By comparing the amplitudes of the main mode in (3.4) and (3.8), one can obtain

$$\kappa+i\omega=V^{(1)}(Q+2\Theta_{l1})+a^2\tilde{V}_3. \tag{3.13}$$

So long as $\kappa_0+i\omega_0$ is the root of (3.10), in the first approximation for the small amplitude we have

$$[\kappa-\kappa_0+i(\omega-\omega_0)](V^{(1)}Q_1-1)+a^2\tilde{V}_3=0, \tag{3.14}$$

where Q_1 is the value of $\partial_w Q(w,u)$ at $w=i\omega_0$. From (3.14) we deduce the set of equations

$$\kappa-\kappa_0=-\chi a^2,\quad \omega-\omega_0=-\mu a^2, \tag{3.15}$$

where

$$\chi=\mathrm{Re}(U_0), \tag{3.16}$$

$$\mu=\mathrm{Im}(U_0), \tag{3.17}$$

$U_0=\tilde{V}_3/(V^{(1)}Q_1-1)$, and Im implies the "imaginary part." the system under consideration for $\chi>0$ achieves a limit cycle with the amplitude $a=a_0$ (1.3). At $\chi<0$, a similar limit cycle with a small amplitude is impossible. The second equality of (3.15) yields the correction to the oscillation frequency value.

Let us now consider the ordinary resonance case, where $p\neq 0$ and the disturbance frequency ν is such that Eq. (3.10)

has the root $w=\kappa_0+i\omega_0$ with $\omega_0\approx\nu$ and a small negative quantity κ_0 which corresponds to the presence of damping. In this case, the value of $\vartheta=\nu t-\varphi(t)$ is approximately constant, and, instead of (3.13), neglecting nonresonant terms one can obtain

$$a(\kappa+i\omega)=aV^{(1)}(Q+2\Theta_{l1})+a^3\tilde{V}_3+pV^{(1)}\Theta_{l0}(\nu)e^{i\vartheta},$$

and, in the first approximation,

$$a[\kappa-\kappa_0+i(\omega-\omega_0)]+a^3(\chi+i\mu)+fe^{i(\vartheta+\psi)}=0, \tag{3.18}$$

where $f=p|U_1|$, $\psi=\arg U_1$, and $U_1=V^{(1)}\Theta_{l0}(\nu)/(V^{(1)}Q_1-1)$.

Replacing κ and ω with the corresponding time derivatives we can write Eq. (3.18) as a set of equations

$$\begin{aligned}\dot{\vartheta}&=(f/a)\sin(\vartheta+\psi)+\delta+\mu a^2,\\ \dot{a}&=(\kappa_0-a^2\chi)a-f\cos(\vartheta+\psi),\end{aligned} \tag{3.19}$$

where the detuning $\delta=\nu-\omega_0$ is small. Equation (3.18) permits us to calculate κ and ω for given a, p, and ϑ, and, on the other hand, the amplitude a and the phase shift ϑ for the limit cycle may be found from (3.18) by substituting $\kappa=0$. For the limit cycle we have

$$\vartheta+\psi=\arg[\kappa_0-a^2\chi+i(\omega_0-\nu-a^2\mu)]$$

and Eq. (1.5).

Equations (3.19) may be used for the stability analysis of points in the resonance curve (1.5). At the stationary point we have

$$\begin{aligned}\sin(\vartheta+\psi)&=-(a/f)(\delta+\mu a^2),\\ \cos(\vartheta+\psi)&=(a/f)(\kappa_0-a^2\chi).\end{aligned} \tag{3.20}$$

For the deviations of the amplitude (Δa) and the phase ($\Delta\vartheta$) from their stationary values a and ϑ, in the linear approximation, from Eqs. (3.19), in view of Eqs. (3.20), we arrive at

$$\begin{aligned}\Delta\dot{a}&=(\kappa_0-3\chi a^2)\Delta a-(\delta+\mu a^2)a\Delta\vartheta,\\ \Delta\dot{\vartheta}&=(\delta+3\mu a^2)(\Delta a/a)+(\kappa_0-\chi a^2)\Delta\vartheta.\end{aligned} \tag{3.21}$$

The proper characteristic equation may be written in the form

$$(\kappa_0-\chi a^2-\lambda)(\kappa_0-3\chi a^2-\lambda)+(\delta+\mu a^2)(\delta+3\mu a^2)=0, \tag{3.22}$$

where λ is the characteristic exponent whose negativeness (or negativeness of its real part) indicates the stability. As follows from (3.22), the stationary point (3.20) is stable if

$$\{(\kappa_0-\chi a^2)(\kappa_0-3\chi a^2)+(\delta+\mu a^2)(\delta+3\mu a^2)>0,\quad \kappa_0<2\chi a^2\}. \tag{3.23}$$

If R is small, $\beta<1/2$, and $\alpha\approx(1-\beta)^{-1}$, the self-sustained oscillation frequency is low, and the obtained limit-cycle amplitude value (1.3) may be compared with the one obtained by Kurtze in Ref. 10. Simple but cumbersome calculations have given the expression for the amplitude, which would correspond to the one given by the first term of expansion (4.22) in Ref. 10 if formula (3.14c) in Ref. 10 for the parameter denoted there as g is replaced (in the notation of Ref. 10) by the formula

$$g=\{l^2[2\alpha_{-3}+\beta(1-\beta)(1-5\beta)]+(1-\beta)a\delta_c\}[\beta(2-3\beta)]^{-1}+(af/2),$$

which, in fact, may be obtained during the transformation of (3.11) to (3.13) in Ref. 10.

In the case of a parametric resonance [$\nu\approx2\omega_0$ and $\theta=\nu t-2\varphi(t)$ is approximately constant], the external force term in (3.18) takes the form $paV^{(1)}\Theta_{l1}(\nu)e^{i\theta}$, so (3.18) and (3.19) are replaced by the equations

$$\begin{aligned}\kappa-\kappa_0+i(\omega-\omega_0)+a^2(\chi+i\mu)+ge^{i(\theta+\psi)}&=0,\\ \dot{\theta}&=2[f\sin(\theta+\psi)+\delta+\mu a^2],\\ \dot{a}&=[\kappa_0-a^2\chi-g\cos(\theta+\psi)]a,\end{aligned} \tag{3.24}$$

where $\delta=(\nu/2)-\omega_0$, $g=p|U_2|$, $\psi=\arg U_2$, and $U_2=V^{(1)}\Theta_{l1}(\nu)/(V^{(1)}Q_1-1)$. Finally, the equation of the resonance curve for parametric resonance takes the form

$$(\delta+\mu a^2)^2+(\kappa_0-\chi a^2)^2=g^2 \tag{3.25}$$

[compare with Eq. (1.5)]. The stationary point stability analysis, similar to that of Eqs. (3.19), yields the following stability conditions:

$$\{a^2(\mu^2+\chi^2)>\kappa_0\chi-\mu\delta,\quad \kappa_0<2\chi a^2\} \tag{3.26}$$

[cf. conditions (3.23)].

IV. RESONANCE CURVE ANALYSIS

The behavior of the resonance system somewhat differs in the two cases under study. The corresponding resonance curves on the (δ,a^2) plane are shown in Figs. 3 and 4, where $\mu>0$ is supposed (the change of μ to $-\mu$ implies reflection of the curves with respect to the axis $\delta=0$).

Let us first discuss the features of the ordinary, main-mode resonance curves [see Figs. 3(a)–3(d), where different curves correspond to different f values]. Their shapes depend on the signs of $\mu^2-3\chi^2$ and $\kappa_0\chi$ values.

If $\mu^2<3\chi^2$ and $\kappa_0\chi<0$, the curves of (1.5) have no vertical-tangent points (VTP's) for any given f, and there is only one a^2 value for any δ [see Fig. 3(a)], so the oscillation amplitude is unambiguously determined by the external-force frequency at the fixed external-force amplitude.

If $\mu^2>3\chi^2$ and $\kappa_0\chi<0$, then for $f>f_3$, where

$$f_3^2=(\chi^2+\mu^2)[2\kappa_0/(\chi\sqrt{3})]^3(\sqrt{3}-|\mu/\chi|)^{-3}, \tag{4.1}$$

there are two VTP's in the curve, and between these tangents each value of δ corresponds to three values of a^2 [see Fig. 3(b)]. This means that for a fixed external-force amplitude with $f>f_3$ the oscillation amplitude changes abruptly with continuous frequency variation. For the example illustrated by Fig. 3(b), with a frequency detuning increase up to $\delta=\delta_A$, the oscillation amplitude changes continuously, but on passing through this point the oscillation amplitude changes abruptly to its new (greater) value and further it changes continuously; on the other hand, with a frequency decrease,

the abrupt change of oscillation amplitude takes place at $\delta=\delta_B$, so (δ_B,δ_A) is here the interval of bistability, i.e., depending on the frequency change direction there may be two different amplitude values for a given $\delta\in(\delta_B,\delta_A)$; the third value, which is defined by a point in the curve between the points A and B, corresponds to oscillations unstable in the linear approximation.

If $\kappa_0\chi>0$ and $f<f_2$, where

$$f_2^2=4\kappa_0^3/(27\chi), \tag{4.2}$$

the curve consists of two parts [see Figs. 3(c) and 3(d)]. In the presence of a very small disturbance with its associated frequency, the system may oscillate with the amplitude a close to a_0 (1.3) (upper branch), or with a very small amplitude (lower branch). The sequence of changes in a curve of this kind depends on the sign of $(\mu^2-3\chi^2)$. For a small f [more precisely, for $f<\min(f_1,f_2)$] there are no VTP's in the lower branch.

If $\mu^2<3\chi^2$ (in addition to $\kappa_0\chi>0$), then up to the linkage of the branches, the VTP's [in contrast to Fig. 3(d)] are only in the upper branch [see Fig. 3(c)]. At $f=f_2$ (4.2) the branches link, the tangents at the linkage point are sloping towards different sides with respect to the vertical, and after that an additional pair of VTP's appears, providing two intervals of bistability. Further, as f increases and reaches successively the values $f=f_1$ and $f=f_3$, where

$$f_1^2=(\chi^2+\mu^2)[2\kappa_0/(\chi\sqrt{3})]^3(\sqrt{3}+|\mu/\chi|)^{-3}, \tag{4.3}$$

the intervals of bistability successively disappear.

If $\mu^2>3\chi^2$ (and $\kappa_0\chi>0$) and f increases and reaches the value $f=f_1$ (before the branch linkage, because $f_1<f_2$ here), the pair of VTP's appears in the lower branch and so a second interval of bistability arises [see Fig. 3(d)]. At the branch linkage both tangents at the linkage point are sloping towards the same side with respect to the vertical and the bistability intervals merge into one, which does not disappear with a further f increase.

Now let us discuss the features of the parametric resonance (PR) curves [see Figs. 4(a) and 4(b), where different curves correspond to different g values]. The PR amplitude may be nonzero only in a restricted interval of detuning.

If $\kappa_0<0$ and $\chi>0$ [see Fig. 4(a)], the PR may take place only for $g>g_0$, where

$$g_0=|\kappa_0|, \tag{4.4}$$

rather than for any arbitrary small external-force amplitude. With further increase in g to g_1, where

$$g_1=|\kappa_0|\sqrt{1+(\chi/\mu)^2}, \tag{4.5}$$

VTP's in the resonance curve appear [see point B in Fig. 4(a)]; after that the frequency interval emerges in which for every value of detuning there are two values of amplitude [(δ_B,δ_C) in Fig. 4(a)]. The smaller a^2 value corresponds to oscillations unstable in the linear approximation while the greater a^2 corresponds to stable ones. The resonance oscillation amplitude depends on the direction of the external-force frequency change (at fixed amplitude), at which the operating point is reached. For example, in the case of the curves shown in Fig. 4(a), with decreasing frequency, the oscillations arise at the detuning $\delta=\delta_A$ and their amplitude changes continuously, but at $\delta=\delta_B$ the resonance oscillations disappear abruptly. However, with increasing frequency the oscillations arise at $\delta=\delta_C$ with finite amplitude, which continuously decreases to zero at $\delta=\delta_A$.

If $\kappa_0>0$ and $\chi>0$ [see Fig. 4(b)], then the oscillations with amplitude $a=a_0$ (1.3) arise even without external perturbation. When g rises to g_0, the PR curve is tangent to the axis $a^2=0$. After that two intervals of bistability arise: (δ_D,δ_E) and (δ_F,δ_G) in Fig. 4(b). With increase or decrease in the external-force frequency at a fixed amplitude, the resonance oscillations either appear or disappear abruptly, having finite amplitude. With a further increase of g to g_1 (4.5) one of the bistability intervals disappears and on this side of the curve the oscillation amplitude continuously comes to zero with frequency increase.

With the simultaneous change of χ and κ_0 to $-\chi$ and $-\kappa_0$, formally, the resonance curve does not change, but the stability of the operating points in it does. The first inequalities in conditions (3.23) and (3.26) are valid at all points in the resonance curves except those which correspond to the second (in descending order) root (a^2) of the resonance curve equation (1.5) or (3.25) for a given δ. The instability of such points is common for resonance systems.[5,6] The second inequality in (3.23) and (3.26) may be considered as generalization to the case $\chi<0$ of the typical stability condition $\kappa_0<0$ which takes place at $\chi\neq0$.

So, if $\kappa_0>0$ and $\chi>0$, then the lower part of the PR curve, the lower part of the upper branch of the ordinary resonance curve, and all points with $a<a_2$ where

$$a_2=\sqrt{\kappa_0/(2\chi)} \tag{4.6}$$

correspond to unstable oscillations and the rest of the operating points are stable. If $\kappa_0<0$ and $\chi<0$, then the operating points with $a>a_2$ for both types of resonance become unstable. If $\kappa_0>0$ and $\chi<0$, then all points in the resonance curves considered become unstable. The horizontal line in Figs. 3(c), 3(d), and 4(b) corresponds to the amplitude level $a=a_2$.

To calculate the values of μ, χ, and κ_0 from the experimental resonance curves on the (δ,a^2) plane, we may propose the following prescription. Having the curves for different f or g and drawing the OM line (see Figs. 3 and 4) through the points at which the tangent is horizontal ($\delta=-\mu a^2$), one would obtain a straight line, the slope of which determines μ, and the intersection with the axis $a^2=0$ determines the frequency at which $\delta=0$ (i.e., $\nu=\omega_0$ or $\nu=2\omega_0$, respectively).

In the PR case, the ratio of those values of g for which the points with vertical and horizontal tangents come to the axis $a^2=0$ is equal to $\sqrt{1+(\chi/\mu)^2}$, so, when measuring this ratio in an experiment, one may calculate the value of $|\chi/\mu|$. Moreover, for the VTP's on the $a^2=0$ axis the equality $\kappa_0=\mu\delta/\chi$ holds. It may then be used to obtain κ_0.

In the case of ordinary resonance, the $|\chi/\mu|$ value can also be obtained from the ratio of f values corresponding to the linkage of branches [f_2 (4.2)] and to the appearance and disappearance of the bistability intervals [f_1 (4.3) and f_3 (4.1)]. Moreover, the equality $\kappa_0=-3\chi\delta/\mu$ for κ_0 at the linkage point is valid.

V. SPATIAL INHOMOGENEITY OF HEAT REMOVAL

Another possible way to investigate the resonant phenomena associated with the oscillatory motion of the EC front is to consider its propagation in specially prepared thin amorphous films with spatial periodicity of their thickness. Such films can be prepared, for example, by making wavy the surface of a substrate before film deposition.

We consider the case where the laser is absent $[P_0(x)=0]$, so the average front velocity is not fixed, and the expansion of the function $s(t)$ takes the form [compare with (3.1)]

$$s(t)=\bar{s}(t)+\mathrm{Re}(ae^{i\varphi}+a^2\tilde{B}_2e^{2\varphi i}+\cdots), \tag{5.1}$$

where $d\bar{s}/dt=\bar{v}$ is approximately constant. Moreover, $\bar{v}\approx v_0$, where v_0 is the root of the set of equations

$$v_0=V(T_0), \quad T_0=\Theta_c(v_0). \tag{5.2}$$

It may be written

$$\bar{v}=v_0+a^2\bar{V}_2+\cdots, \tag{5.3}$$

where the coefficient $\bar{V}_2$ is found from the harmonic balance condition [see (5.9) below]. Expansion (5.1) implies the expansion

$$v(t)=\bar{v}+\mathrm{Re}[(\kappa+i\omega)ae^{i\varphi}+2(\kappa+i\omega)a^2\tilde{B}_2e^{2\varphi i}]+\cdots. \tag{5.4}$$

If the oscillation amplitude a is small and there is no disturbance, the expansion of the right-hand side of (2.4) yields in this case

$$T(s(t),t)=\bar{T}+\mathrm{Re}\{ae^{i\varphi}Q(\kappa+i\omega,\bar{v})+a^2e^{2i\varphi}\tilde{\Theta}_2+a^3e^{i\varphi}\tilde{\Theta}_3+\cdots\}, \tag{5.5}$$

$$\bar{T}=T_0+a^2\bar{\Theta}_2+\cdots, \tag{5.6}$$

where $\bar{\Theta}_2=\bar{A}_t+\Theta_c^{(1)}\bar{V}_2$, $\tilde{\Theta}_3=\tilde{B}_2\tilde{F}_3+\tilde{A}_3$, $\tilde{\Theta}_2=\tilde{B}_2Q(2i\omega,v_0)+\tilde{A}_2$, and the notation introduced in Sec. III is used.

The expansion of the function $V(T)$ near the steady-state point taking into account (5.5) gives

$$V(T(s(t),t))=v_0+a^2(V^{(1)}\bar{\Theta}_2+\bar{A}_v)+\cdots+\mathrm{Re}\{e^{i\varphi}[aV^{(1)}Q+a^3\tilde{V}_3]+e^{2\varphi i}a^2[V^{(1)}\tilde{\Theta}_2+\tfrac{1}{4}V^{(2)}Q^2]+\cdots\}, \tag{5.7}$$

where Q_2 is the value of $\partial_vQ(i\omega_0,v)$ at $v=v_0$,

$$\bar{A}_v=\tfrac{1}{4}V^{(2)}|Q|^2,$$

and

$$\tilde{V}_3=V^{(1)}(\tilde{\Theta}_3+Q_2\bar{V}_2)+V^{(2)}[\tfrac{1}{2}\tilde{\Theta}_2Q^*+\bar{\Theta}_2Q]+\tfrac{1}{8}V^{(3)}Q^2Q^*,$$

in this case.

As a consequence of (5.4) and (5.7), the weakly anharmonic oscillations under consideration would take place for the v_0 and T_0 values [satisfying (5.2)] for which the equation

$$w=V^{(1)}(T_0)Q(w,v_0) \tag{5.8}$$

has the root $w=\kappa_0+i\omega_0$ with $\kappa_0\ll\omega_0$. Further, comparison between the amplitudes of the double-frequency terms and nonoscillating terms in (5.4) and (5.7) yields

$$\bar{V}_2=\frac{V^{(1)}\bar{A}_t+\bar{A}_v}{1-V^{(1)}\Theta_c^{(1)}}, \quad \bar{\Theta}_2=\frac{\Theta_c^{(1)}\bar{A}_v+\bar{A}_t}{1-V^{(1)}\Theta_c^{(1)}}, \tag{5.9}$$

$$\tilde{B}_2=[V^{(1)}\tilde{A}_2+\tfrac{1}{4}V^{(2)}Q^2][2i\omega_0-V^{(1)}Q(2i\omega_0,v_0)]^{-1}.$$

These formulas, together with (5.1), (5.3), and (5.6), give the corrections to the steady-state values and the double-frequency amplitude, if the main-mode amplitude is given.

Let $\gamma\neq0$, and the disturbance wave number k be such that Eq. (5.8) has the root $w=\kappa_0+i\omega_0$ with $\omega_0\approx kv_0$ and small negative κ_0. In this case, the value of $\vartheta=k\bar{s}(t)-\varphi(t)$ is approximately constant, and one can obtain Eqs. (3.18), (3.19), and (1.5), in which $f=\gamma|U_1|$, $U_1=V^{(1)}H/(V^{(1)}Q_1-1)$, and ν is replaced by $k\bar{v}$. Here

$$H=(T_0/q_1)(q_0+q_1)/[(q_0+q_1)^2+k^2],$$

where $q_0=\sqrt{1+(v_0/2)^2}$ and $q_1=\sqrt{1+(v_0/2)^2+ikv_0}$.

If the disturbance wave number k is such that $kv_0\approx2\omega_0$, then the value of $\theta=k\bar{s}(t)-2\varphi(t)$ is approximately constant and one arrives at Eqs. (3.24) and (3.25), in which $g=\gamma|U_2|$, $U_2=V^{(1)}H_2/(V^{(1)}Q_1-1)$, ν is replaced by $k\bar{v}$, and

$$H_2=-(v_0^2/8)(q_++q_0)\{q_+q_0[(q_++q_0)^2+k^2]\}^{-1}+(v_0/8)\times(v_0-ik)(q_++q_-)\{q_+q_-[(q_++q_-)^2+k^2]\}^{-1}+ikv_0(4q_+)^{-1}\{[(q_++q_-)^2+k^2]^{-1}-[(q_++q_0)^2+k^2]^{-1}\},$$

where $q\pm=\sqrt{1+(v_0/2)^2\pm(ikv_0/2)}$; χ and μ are defined by formulas (3.16) and (3.17), as above.

Having arrived at Eqs. (1.5) and (3.25) we may repeat the results of Sec. IV in the resonance curve analysis.

Let us now relate our results obtained, as was pointed out in the Introduction, for all frequencies (but small amplitudes) to the results of van Saarloos and Weeks[4] near the point $\alpha=3$, $\beta=\frac{2}{3}$. In the neighborhood of this point (where the ''kinetic curve'' and the ''heat removal curve'' are nearly tangent and the frequency of oscillations is small) one approximately gets

$$\chi=\frac{135}{2}\left(1-\frac{V''}{18}\right)\left(\frac{V''}{18}-\frac{3}{5}\right),$$

where V'' is the value of $[(T-T_s)^2/V]d^2V/dT^2$, so that $\chi>0$ occurs for $V''/18\in(\frac{3}{5},1)$. It should be pointed out that 18 is the value of V'' at the corresponding point which has the function $v=V_c(T)$, being the inverse of the function $T=T_s+\Theta_c(v)$, and the inequality $\kappa_0>0$ occurs if the steepness of the ''kinetic curve'' is greater than that of $V_c(T)$. Near the mentioned point, the calculated amplitude of the limit cycle would correspond to the value which may be obtained by the method of Ref. 4 in the vicinity of the $5\delta\alpha\approx18\delta\beta$ line, where $\delta\alpha=\alpha-3$ and $\delta\beta=\beta-\frac{2}{3}$ are supposed small. There the unperturbed growth factor $\kappa_0\approx5\delta\alpha-18\delta\beta$ is small in comparison with the frequency $\omega_0\approx\sqrt{24(9\,\delta\beta-\delta\alpha)}$ and the limit-cycle amplitude is determined by the equality

$$(\dot{V}/V_{ss})_{\max} = -4\lambda_2\lambda_1^2/(a_1 a_2) \tag{5.10}$$

(in the notation of Ref. 4), where $\lambda_1 = 24(\delta\alpha - 9\delta\beta)$, $\lambda_2 = 10\delta\alpha - 36\delta\beta$, $a_1 = 4(V'' - 18)$, and $a_2 = 60(V''/18 - \frac{3}{5})$ (here the a_2 value is obtained taking into account the corrections mentioned in Refs. 4 and 9). The left-hand side of (5.10), in our notation, is equal to $(\omega_0^2 a/v_0)^2$, where $v_0 \approx 2\sqrt{2}$, and the right-hand side of (5.10) is equal to $\kappa_0\omega_0^4/(8\chi)^2$, so one arrives at the equality $a^2 = \kappa_0/\chi$, as it should be.

VI. BISTABILITY AREA ANALYSIS

The results of the linear stability analysis,[4] combined with the results of the stationary analysis for the typical kinetic curve (2.3), offer additional details for the quasisteady stability picture that was presented in Ref. 2. Let us briefly outline some results of Ref. 2. We now consider the case of self-sustained crystallization without a driving laser or any external perturbation. The stationary regime is determined by the intersection of the kinetic curve $v = V_s \exp(-E/T)$ and the heat removal curve $T = T_s + \Theta_c(v)$. For the curve-tangency case the additional equality $EF(v/2) = T^2$ has to take place at the curve-tangency point [here we introduce the function $F(\xi) = \xi(1+\xi^2)^{-3/2}$, which corresponds to the one used in Ref. 2 in the relaxation-type heat removal case]. For a fixed E, the set of T_s and V_s values at which the curves are tangent forms a curved line on the (T_s, V_s) plane. This curved line may be obtained from the above-written three equalities by the use of v as a parameter and calculation of T, T_s, and V_s by the formulas

$$T = \sqrt{EF(v/2)}, \quad T_s = T - \Theta_c(v), \quad V_s = v\ \exp(E/T). \tag{6.1}$$

To ensure $T_s > 0$, the v value has to obey the inequality $v < v_m$, where $v_m = E2\sqrt{2}/(1+\sqrt{1+4E^2})^{1/2}$.

Differentiating the right-hand side of the equality

$$T_s = \sqrt{EF(v/2)} - \Theta_c(v) \tag{6.2}$$

with respect to v for a fixed E, one can find the derivative to be equal to zero for $v = v_c$, where $v_c = v_c(E)$ is the root of the equation

$$2 - v_c^2 = 2[v_c^2(4+v_c^2)/E^2]^{1/4}.$$

Earlier [see the text before formula (2.1)], we took c/Γ and $\sqrt{\lambda/\Gamma}$ as units of time and coordinate, so the unit of velocity is $(\sqrt{\lambda\Gamma}/c)$. Hence the increase in the film thickness corresponds to a decrease in Γ and hence to an increase of the dimensionless parameter V_s. Thus we can consider V_s as a quantitative measure of the film thickness and present the stability picture[2] on the (T_s, V_s) plane (in Fig. 5, a logarithmic scale along the V_s axis is used).

Those (T_s, V_s) plane points that correspond to the cases where the kinetic curve and the heat removal curve are tangent form a curved line consisting of two smooth parts tangent in the common point: the upper, V_s^-, for which $v \in (0, v_c)$, and the lower, V_s^+, for which $v \in (v_c, v_m)$. According to the stationary consideration,[2] the region between these parts corresponds to bistability: for $V_s < V_s^+$ the only possible regime is slow crystallization and for $V_s > V_s^-$ explosive crystallization, and the region of bistability admits two different stationary regimes: slow and explosive.

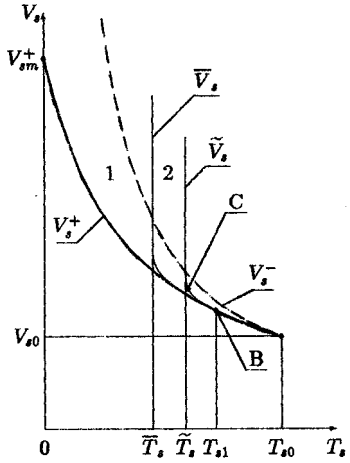

FIG. 5. The quasisteady stability (T_s, V_s) diagram for the Arrhenius-type $V(T)$ curve (2.3) with $E = 33.3$ [typical of the known explosively crystallized materials (Ref. 2)]; the dimensionless variables T_s and V_s are related to the temperature of the substrate and the film thickness d_s ($V_s \sim d_s^{1/2}$), respectively; a logarithmic scale along the V_s axis is used: for the present case the $\ln V_{s0}$ and $\ln V_{sm}^+$ values obtained from equalities (6.1) are equal to 8.88 and 35.6, respectively; the diagram is modified as compared with Fig. 9 in Ref. 2 by taking into account the results of the dynamic stability analysis. The points between the curves V_s^- and V_s^+ belong to the region of steady-state bistability, discussed in Ref. 2: for any point in it there are two possible stable values of the constant front velocity. In regions 1 (between the curves V_s^+ and $\bar{V}_s$) and 2 (between the curves $\bar{V}_s$ and $\tilde{V}_s$) the explosive crystallization regime is unstable (monotonic and oscillatory, respectively). The curves $\bar{V}_s$ and $\tilde{V}_s$ originate from point B (this corresponds to zero frequency oscillations) and asymptotically (at $V_s \to \infty$) come to the lines $T_s = \bar{T}_s$ and $T_s = \tilde{T}_s$, respectively. The part BC of the stability boundary $\tilde{V}_s$ corresponds to hard excitation of oscillations and the other part of $\tilde{V}_s$ corresponds to soft excitation; the coordinate of point C can be determined from the condition $\chi = 0$. The symbols $\bar{T}_s$, $\tilde{T}_s$, T_{s1}, and T_{s0} are introduced by relations (6.3)–(6.5).

However, the linear stability analysis[3,4] shows that for $T_s < T_{s1}$ (defined below) the points slightly higher than those in the V_s^+ branch correspond to a linearly unstable explosive regime. Moreover, the instability is monotonic up to the $\bar{V}_s$ curve, above which it becomes oscillatory. The steady-state explosive regime becomes linearly stable only for $V_s > \tilde{V}_s$. The curves $\bar{V}_s$ and $\tilde{V}_s$ are defined by the equalities $\beta = (1+\alpha)^2/(8\alpha)$ and $\beta = (\alpha^2 - 1)/(4\alpha)$, respectively. Taking into account that $v = 2\sqrt{\beta/(1-\beta)}$ and $\alpha = (T - T_s)E/T^2$, for our heat removal curve and kinetic curve we can estimate T_s and V_s on the curved lines $\bar{V}_s$ and $\tilde{V}_s$ by the formulas

$$T_s = \sqrt{E\Theta_c(v)/\alpha} - \Theta_c(v), \quad V_s = v\ \exp[\sqrt{E\alpha/\Theta_c(v)}],$$

where the v value is determined by α, through the values of β from the corresponding equalities. To ensure $T_s > 0$, the inequality $\alpha\sqrt{\beta} < E$ must be fulfilled. The T_{s1} value corresponds to the point $\alpha = 3$, $\beta = \frac{2}{3}$, so

$$T_{s1}=(E\sqrt{2/27})^{1/2}-\sqrt{2/3}. \tag{6.3}$$

The T_{s0} value corresponds to the point where the mentioned derivative of T_s (6.2) with respect to v changes sign, so

$$T_{s0}=\sqrt{4Ev_c(4+v_c^2)^{-3/2}}-v_c(4+v_c^2)^{-1/2}. \tag{6.4}$$

The $\tilde{T}_s$ and $\bar{T}_s$ values are related to the points at which $\beta=1$, i.e., $v\to\infty$ for them, so

$$\tilde{T}_s=\sqrt{E/\tilde{\alpha}}-1, \quad \bar{T}_s=\sqrt{E/\bar{\alpha}}-1, \tag{6.5}$$

where $\tilde{\alpha}=2+\sqrt{5}$ and $\bar{\alpha}=3+2\sqrt{2}$. To ensure positive values of T_{s1}, $\tilde{T}_s$, and $\bar{T}_s$ determined above, the E value has to exceed $\sqrt{6}$, $2+\sqrt{5}$, and $3+2\sqrt{2}$, respectively.

If we fix T_s and seek the thickness corresponding to the given front velocity value, which continuously increases, the operating point in the (T_s,V_s) plane will first move along the $T_s=$const line from the $V_s=0$ axis to the line V_s^-, then come to the V_s^+ line, and then go to infinity. So for any point between the V_s^+ and V_s^- lines there are three possible values of the front velocity. From the quasisteady consideration it seems that only regimes with an intermediate velocity value are unstable. However, the linear consideration indicates the instability of EC regimes, too, for the points situated in regions 1 and 2 in Fig. 5. Moreover, in region 1 the instability is monotonic and in region 2 it is oscillating. These regions are restricted by the lines which start at the point B (see Fig. 5) and asymptotically come to the straight lines $T=T_s$ and $T=\tilde{T}_s$, respectively. The analysis made in Sec. V reveals how nonlinearity influences the stability of oscillations of a small but finite amplitude for the points near the line that restricts region 2 on the greater-T_s side. The analysis of the expression for χ (3.16) in the case of a kinetic dependence of the form (2.3) shows that at the origin of the mentioned line (near point B) the variable χ is negative, so to the right of the line oscillations with a very small amplitude are damped. But if the oscillations have previously been excited with an amplitude greater than a certain value (which is small if the distance from the line is small), the oscillations build up; and to the left of the line the oscillations build up and a limit cycle with an arbitrarily small amplitude near the line is impossible. This situation takes place throughout the length of the line considered (the right boundary of the oscillatory unstable regimes) if the variable E does not exceed some value E_0 ($E_0\approx17.5$) which is the root of some equation (squared with respect to $E^{-1/2}$) whose coefficients may be obtained with the limit transition $v\to\infty$ in the expression for $\tilde{V}_3$ (3.9) and in the expressions for the variables entering into the right-hand side of (3.9). But if $E>E_0$, then the point C in the line appears (see Fig. 5 drawn for $E=33.3$), above which the situation described changes to its opposite: the points to the right of the line become stable to small-amplitude perturbations (if the distance from the line is small), and for the points to the left of the line the oscillations have a limit cycle whose amplitude is defined by Eq. (1.3). If $E\to E_0$, point C moves to infinity.

From the experimental data on known explosively crystallized materials (Table 1 of Ref. 2) it follows that for most cases observed $E\sim30-40$, so we have $v_c^2\approx2$, $T_s/T_{s0}\approx0.666$, $\tilde{T}_s/T_{s0}\approx0.784$, and $T_{s1}/T_{s0}\approx0.84$.

The essential narrowing of the interval (on the T_s axis) of stable explosive regimes may be considered as a possible explanation of the difficulty of observing explosive crystallization in systems with intensive heat removal, for example, in films on a good heat-conducting material such as sapphire.

VII. SUMMARY

The main final results of our paper are Eqs. (1.5) and (3.25), and the expressions for μ and χ [see formulas (3.17) and (3.16)] in terms of the kinetic and thermophysical parameters of our model. The graphic analysis of the formulas is presented in Figs. 3(a)–3(d) (where the external-force frequency is $\nu\approx\omega_0$) and in Figs. 4(a) and 4(b) (parametric excitation of the main harmonics with the frequency $\nu\approx2\omega_0$). We have also analyzed the stability of the points determined by Eqs. (1.5) and (3.25). Depending on the external-force value and the values of the parameters μ and χ, the resonance curves on the plane (δ,a^2) exhibit different behavior, from simple resonance curves [Fig. 3(a)] to more complex curves with bistability and hysteresis [Figs. 3(b)–3(d), 4(a) and 4(b)] and disconnected parts [Figs. 3(c) and 3(d)]. In our opinion, it would be of interest to observe this behavior in real experimental situations. At the end of Sec. IV we have also described some simple prescriptions for extracting the values of μ, χ, and κ_0 from the experimental resonance curves in order to check the results obtained in our relatively simple model of EC front propagation.

We have compared a part of our results (the region of low-frequency oscillations) with the corresponding results presented in Refs. 4 and 10. At the end of the paper we have also discussed the EC stability diagram with due account of the results of the linear stability analysis.

In conclusion, it should also be mentioned that nonisothermal effects similar to explosive crystallization of glasses may also be observed in the decay of other structurally frozen metastable phases (for example, in liquid crystals[11] or polymers[12]). In our phenomenological approach such different substances are characterized only by different interface kinetics, i.e., a specific dependence of the local phase boundary velocity on its temperature [see (2.2)]. So we hope that our results describing the resonance response of the self-sustained nonisothermal periodic front motion may be applied not only to amorphous films but also to a broader class of structurally frozen metastable phases.

APPENDIX

The expressions for $\bar{A}_t$, $\tilde{A}_2$, $\tilde{F}_3$, and $\tilde{A}_3$ [see formulas (3.5) and (3.6)] may be written as follows:

$$\bar{A}_t=v\left(1+\frac{v^2}{2}\right)S_2\left(\sigma,\frac{\omega}{2}\right)-\frac{3}{4}v\omega S_1(\sigma,\omega),$$

$$\tilde{A}_2=-v\left(1+\frac{v^2}{2}\right)S_2\left(\sigma+i\omega,\frac{\omega}{2}\right)+\frac{3}{2}v\omega S_1\left(\sigma+\frac{3}{2}i\omega,\frac{\omega}{2}\right),$$

$$\tilde{F}_3=-\frac{3}{2}v\omega\left[S_1\left(\sigma+i\frac{\omega}{2},\frac{3}{2}\omega\right)+S_1\left(\sigma+\frac{3}{2}i\omega,\frac{\omega}{2}\right)\right]$$
$$+2v\left(1+\frac{v^2}{2}\right)\left[S_2\left(\sigma+i\frac{\omega}{2},\frac{3}{4}\omega\right)-S_2\left(\sigma+i\frac{\omega}{2},\frac{\omega}{4}\right)\right],$$

$$\tilde{A}_3 = -i\frac{\omega^2}{4}\left[S_1\left(\sigma + i\frac{\omega}{2}, \frac{3}{2}\omega\right) + 3S_1\left(\sigma + \frac{3}{2}i\omega, \frac{\omega}{2}\right)\right]$$
$$+ i\frac{\omega}{2}(1+2v^2)\left[S_2\left(\sigma, \frac{\omega}{2}\right) + 2S_2\left(\sigma + i\omega, \frac{\omega}{2}\right)\right]$$
$$- i\frac{v^2}{2}(3+v^2)S_3\left(\sigma + i\frac{\omega}{2}, \frac{\omega}{2}\right),$$

where

$$S_m(\sigma,\omega) = \int_0^\infty \frac{e^{-\sigma\tau}}{2\sqrt{\pi\tau}} \sin^m(\omega\tau)\, d\tau,$$

that is,

$$S_1(\sigma,\omega) = \frac{\omega}{2\sqrt{2}}\left[(\sigma^2+\omega^2)(\sigma+\sqrt{\sigma^2+\omega^2})\right]^{-1/2},$$

$$S_2(\sigma,\omega) = \omega^2(3\sigma^2+16\omega^2)\left[\sqrt{\sigma(\sigma^2+4\omega^2)}(\sigma^2+8\omega^2+\sigma\sqrt{\sigma^2+4\omega^2})\right]^{-1}\left[2\sqrt{\sigma^2+4\omega^2}+(2\sigma^2+2\sigma\sqrt{\sigma^2+4\omega^2})^{1/2}\right]^{-1},$$

$$S_3(\sigma,\omega) = \frac{3}{\sqrt{2}}\,\omega^3\left\{\sigma + \frac{3\sigma^4+30\sigma^2\omega^2+91\omega^4}{(\sigma^2+\omega^2)^{3/2}+(\sigma^2+9\omega^2)^{3/2}}\right\}\left\{\left[(\sigma^2+\omega^2)(\sigma+\sqrt{\sigma^2+\omega^2})\right]^{1/2}+\left[(\sigma^2+9\omega^2)(\sigma+\sqrt{\sigma^2+9\omega^2})\right]^{1/2}\right\}^{-1}$$
$$\times\left[(\sigma^2+\omega^2)(\sigma+\sqrt{\sigma^2+\omega^2})(\sigma^2+9\omega^2)(\sigma+\sqrt{\sigma^2+9\omega^2})\right]^{-1/2}.$$

[1] G. H. Gilmer and H. J. Leamy, *Laser and Electron-Beam Processing of Materials* (Academic, New York, 1980), p. 227.

[2] V. A. Shklovskij and V. M. Kuz'menko, Sov. Phys. Usp. **32**, 163 (1989).

[3] V. A. Shklovskij, Sov. Phys. JETP **55**, 311 (1982).

[4] W. van Saarloos and J. D. Weeks, Physica D **12**, 279 (1984).

[5] L. D. Landau and E. M. Lifshits, *Mechanics* (Nauka, Moscow, 1988) (in Russian).

[6] B. V. Novogilov, *Nonstationary Burning of Solid Rocket Fuels* (Nauka, Moscow, 1973) (in Russian).

[7] D. A. Kurtze, W. van Saarloos, and J. D. Weeks, Phys. Rev. B **30**, 1398 (1984).

[8] N. N. Bogolubov and Yu. A. Mitropolsky, *Asymptotic Methods in Nonlinear Oscillations Theory* (Nauka, Moscow, 1974) (in Russian).

[9] D. A. Kurtze, Phys. Rev. B **40**, 11 104 (1989).

[10] D. A. Kurtze, Physica D **20**, 303 (1986).

[11] D. L. Uhrich *et al.*, Phys. Rev. A **12**, 211 (1975).

[12] Yu. K. Godovskij, *Thermal Physics of Polymers* (Khimiya, Moscow, 1982) (in Russian).